Robust Control Strategy for Inductive Parametric Uncertainties of DC/DC Converters in Islanded DC Microgrid

Salisu Abdullahi, Tao Jin, and P. M. Lingom

***Abstract*—Direct current (DC) microgrid consists of many parallel power converters that share load currents through the inductance of DC/DC converters. Usually, the inductance parameters are dependent on the physical implementation of the system, and their values may not match their nameplates. Such disparities could lead to unequal response characteristics of the system, which can potentially reduce the performances of the DC microgrid operation. This paper proposes a robust control strategy for inductive parametric uncertainties of DC/DC converters using an optimal control method with integral action. To achieve such a goal, the system model parameters with nominal values are transformed into parametric unmatched uncertainties to form a robust control problem, which is then transformed into a linear quadratic regulator problem. The inductance uncertainties are stabilized with the uncertainty dynamic algebraic Riccati equation (UDARE) using state feedback gain under linear quadratic regulator. The closed-loop control with integral action is adopted to achieve a steady-state error of zero on the DC-link voltage at any uncertainty of the inductive parameter, which subsequently ensures the equal load current sharing. Off-line simulations and real-time validations based on OpalRT have been conducted to demonstrate the effectiveness and robustness of the proposed robust control strategy.**

***Index Terms*—DC/DC converter, DC microgrid, OpalRT, optimal control, parametric uncertainty, robust control.**

NOMENCLATURE

β, μ, φ	Constant design parameters
$\boldsymbol{\Gamma}$	Upper bound matrix component (for unmatched uncertainties)
$\Delta \boldsymbol{V}_u$	Unmatched uncertainty increment
$\Delta i_{k,i-1}$	Current sharing error at sample k
ΔV_o	DC-link voltage error
ΔV_l	Voltage ripple
ΔV_{osh}	DC-link voltage overshoot
ΔV_{op}	DC-link peak voltage
$\Delta \boldsymbol{A}(L_o)$	Converter inductance uncertainty
ξ_k	Integral action variable
λ_i	Current sharing ratio
τ	Upper limit of new variable
Ω	Inductance uncertainty pre-defined bounded set of converters
$\boldsymbol{A} \in \mathbf{R}^{n \times n}$	Nominal system matrix
$\boldsymbol{A}_u \in \mathbf{R}^{n \times n}$	Uncertainty system matrix
$\boldsymbol{B} \in \mathbf{R}^{n \times n}$	Input matrix
$\boldsymbol{B}^+$	Full rank of tall matrix
$\boldsymbol{B}\boldsymbol{B}^+\Delta \boldsymbol{A}$	A matched component
C_{cn}	DC-link capacitance at each converter
C_{fi}	Filter capacitance
C_{fg}	Grid-side filter capacitance
$\boldsymbol{D}$	Upper bound matrix component (for matched uncertainties)
e	Error of DC-link voltage
$\boldsymbol{EM}_{x,ref}$	State references from energy management center
F_s	Switching frequency
$\boldsymbol{H} \in \mathbf{R}^m$	System output vector
$(\boldsymbol{I} - \boldsymbol{B}\boldsymbol{B}^+)\Delta \boldsymbol{A}$	An unmatched component
$\boldsymbol{I} \in \mathbf{R}^{n \times n}$	Identity matrix
$i_{k,i}$	Current pass-through converter inductance at sample k
J_u	Unmatched uncertainty cost function
$\boldsymbol{K}_i$	Integral action gain
$\boldsymbol{K}_u$	Unmatched uncertainty state feedback gain
K_i	Integral gain
K_p	Proportional gain
K_d	Derivative gain
L_n	Nominal converter inductance
L_o	Uncertainty of converter inductance
L_{fi}	Filter inductance
L_{fg}	Grid-side filter inductance
$\boldsymbol{L}_u$	Virtual control input gain
L	Inductance (uncertainty L_o plus nominal L_n) of DC/DC converters

Manuscript received: April 17, 2021; revised: August 8, 2021; accepted: November 3, 2021. Date of CrossCheck: November 3, 2021. Date of online publication: November 30, 2021.

This work was primarily supported by the National Natural Science Foundation of China (No. 51977039).

S. Abdullahi, T. Jin (corresponding author), and P. M. Lingom are with School of Electrical Engineering and Automation, Fuzhou University, Fuzhou, China (e-mail: salisuabdullahisaleh@gmail. com; jintly@fzu. edu. cn; filslingom@yahoo.com).

DOI: 10.35833/MPCE.2021.000241

$\boldsymbol{Q}_u$, $\boldsymbol{R}_u$	Unmatched uncertainty weighting matrices
R_l	Resistive load
$\boldsymbol{S}_u$	Unmatched uncertainty dynamic algebraic Riccati equation (UDARE)
S_i	Converter gate signal
T_s	Sampling time
T	Step-down transformer
t_r	Rising time
t_s	DC-link voltage settling time
$\boldsymbol{u}_k \in \mathbf{R}^m$	Control input
$\boldsymbol{u}_r$	Robust control input
$\boldsymbol{u}_i$	Control input of integral action
$\boldsymbol{u}_{ku}$	Overall control input
$\boldsymbol{u}_{ref}$	Overall control input reference
V_i	Number of distributed energy resources (DERs)
V_o	DC-link voltage
$\boldsymbol{v}_k$	Virtual control input
$\boldsymbol{V}_u(x_k)$	Unmatched uncertainty Lyapunov function candidates
V_{ref}	DC-link voltage reference
$\boldsymbol{x}_k$	State variable
$\boldsymbol{x}_{ref}$	State variable reference
$\boldsymbol{y}_k$	Measured output

I. Introduction

DIRECT current (DC) microgrids have attracted significant attention in recent decades due to their inherent advantages over alternating current (AC) microgrids. In the absence of frequency, DC microgrids are free from skin effect, inrush current problem, or proximity effect [1]. Moreover, the flexible structure of the DC microgrid allows easy integration of distributed energy resources (DERs) such as photovoltaic, fuel cells, and energy storage devices, including batteries and ultracapacitors. A DC load can also be utilized, eliminating the requirement for additional AC/DC power conversion stages [2]-[4]. DC microgrid emerges as an attractive solution not only to supply power to consumers, but also to help them generate and store their own power, and achieve economic benefits locally by injecting power into the AC grid. DC microgrid provides greater advantages in comparison to its AC counterpart, because reactive power management and phase angle synchronization can be avoided. The DC microgrid topology consists of multiple DERs connected to a DC link through parallel DC/DC converters that supply power to a load [5]. The advantages of such a system configuration include reliability, expandability, and maintainability. The primary control objectives of the system are DC-link voltage control and load current sharing. Moreover, real parametric uncertainty is a limitation of the system. This limitation may lead to unequal response characteristics for a wide range of parameter uncertainties during system operation. Different control approaches have been proposed in [6]-[8] to address the aforementioned control issue. Existing solutions are classified mainly according to communication links between parallel DC/DC converters. Different control schemes are required to optimize its performance for each DC/DC converter. Four conventional control structures can be categorized: ① master-slave control; ② centralized control; ③ circular chain control; and ④ average load sharing [6]. Although these control structures have successfully met the control objectives, the communication requirements can cause other issues regarding scalability, flexibility, and liability [7]. In addition, voltage droop control is the most effective method of communicating DERs through current sharing based on their power generation capabilities [8]. However, different approaches are used in the available control schemes to solve DC-link voltage and current sharing problems [9]-[18]. In this paper, a control scheme is presented that controls the DC-link voltage and ensures equal current sharing in DC microgrids to reduce the overall control complexity.

Conventional voltage droop controls with current sharing capabilities have been proposed based on a hierarchical control scheme [9]-[15]. An adaptive droop controller is introduced in [9] in order to eliminate the non-linearity problem. In [10] and [11], a voltage shifting and slope voltage droop adjustment of the distributed secondary control coefficient and current sharing performance have been described. For pilot DC-link voltage regulation with equal current sharing, an average DC-link voltage and current sharing control has been proposed in [12]. A decentralized controller for bounded tracking error of DC-link voltage has been proposed in [13]. The finite control set model predictive control with control input reference derived from virtual capacitance has been previously presented in [14]. According to [15], an event-triggered communication mechanism has been proposed that ensures the accurate current sharing and DC-link voltage regulation simultaneously at the local controller. The decentralized control is proposed for minimizing the DC-link voltage error and for improving DERs resiliency in a DC microgrid cluster [16]. An adaptive droop control has been proposed in [17] in order to improve the current sharing in medium-voltage DC microgrid. Using centralized and decentralized control structures of DC microgrids, robust control against DC source and DC resistive load has been addressed recently [18]. Previously, the effect of inductance parametric uncertainty on DC microgrid has not been investigated in the control scheme presented above. A system with model uncertainty is more realistic and has a greater impact on the practical implementation [19]. For example, as discussed in [20], robustness and adaptability against uncertainty in manufacturing inductance parameters of parallel DC/DC converters in an islanded DC microgrids are the key advantages that robust control could provide compared with other approaches. The uncertainty in inductance parameters could negatively affect the system response characteristics and reduce the overall performances of DC microgrid. Considering the fluctuating nature of inductance parameter resources, it is hard to predict their production that relates to fluctuations constantly [20]. As a result, a robust control strategy is needed to stabilize inductance fluctuation in DC microgrids. This paper proposes a robust control strategy to overcome inductive parametric uncertainties of parallel DC/DC converters in is-

landed DC microgrids. The proposed robust control strategy uses a state feedback mechanism with an optimal control and integral action (OPTCI). An integral action has been added in the state feedback control to ensure zero error on the steady state of DC-link voltage at any uncertainty level of inductance parameter. In order to achieve such a goal, a robust control problem is first formulated and then translated to an optimal control problem using a linear quadratic regulator (LQR). The LQR stabilizes all the states via state feedback control under the uncertainty dynamic algebraic Riccati equation (UDARE). The use of such an approach ensures the stability of the system even under a wide range of parametric uncertainties in the inductance.

The rest of the paper is organized as follows. In Section II, the system modeling and feature analysis considering inductive parametric uncertainties are discussed. Section III provides a detailed description of the proposed robust control strategy. Simulation results using MATLAB/Simulink and OpalRT validation based on hardware-in-the-loop (HIL) using the proposed robust control strategy are provided in Section IV. Finally, the conclusion is presented in Section V.

II. System Modeling and Feature Analysis

Figure 1 shows a typical configuration of an islanded DC microgrid [14]. In this structure, the DC-link voltage is supplied by n DERs through DC/DC converters. There are many DC/DC converters that feed a resistive load through their inductance in the system. A low-pass filter is added at the output of each converter to filter a ripple. PCC is the point of common coupling.

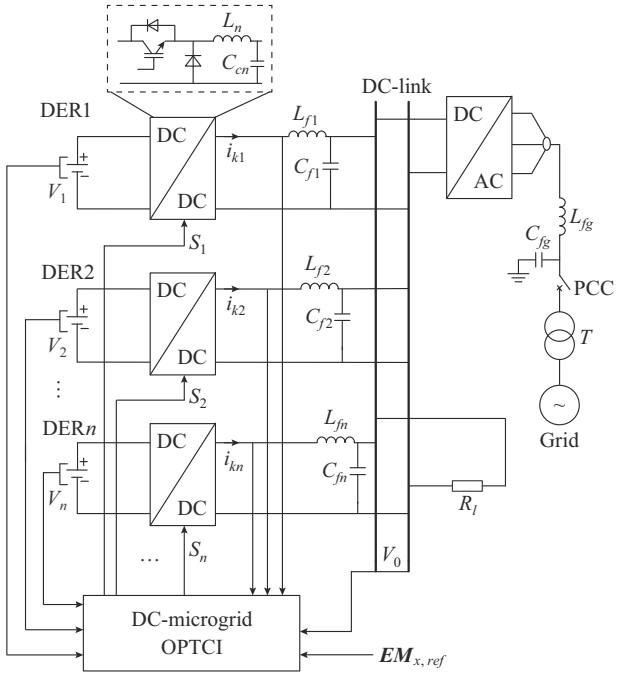

Fig. 1. Typical configuration of an islanded DC microgrid.

The DC microgrid modeling methodology, which includes inductive parametric uncertainty, is described in this section. An analysis of robust control for a wide range of DC/DC converter inductance uncertainties is presented. Initially, the system model is developed based on the nameplate values of all the parameters. Then, the model parametric uncertainty is derived for the inductance uncertainty of the DC/DC converter. DC-link voltage prediction in the nominal system is defined in (1) according to the buck-converter system dynamic in discrete time without consideration of the line impedance [14].

$$V_{o,k+1} = R_l \sum_{j=1}^{n} i_{k+1,j} \tag{1}$$

The current sharing error is computed to ensure equal current sharing between parallel DC/DC converters as follows:

$$\Delta i_{k+1,n-1} = i_{k+1,n-1} - \lambda_{n-1} i_{k+1,n} \tag{2}$$

From (2), the current prediction of the output of the DC/DC converter is generated by:

$$i_{k+1,n} = \frac{(S_n V_n - V_o)T_s}{L_n} + i_{k,n} \tag{3}$$

The current sharing error for n-parallel DC/DC converters in discrete time is provided in (4), which is obtained by inserting (3) into (2).

$$\Delta i_{k+1,n-1} = \frac{(S_n V_n - V_o)T_s}{L_{n-1}} + i_{k,n-1} - \lambda_{n-1}\left[\frac{(S_n V_n - V_o)T_s}{L_n} + i_{k,n}\right] \tag{4}$$

$$\lambda_{n-1} = \frac{i_{k+1,n-1}}{i_{k+1,n}} \tag{5}$$

After an extended mathematical manipulation, the overall n-parallel DC/DC converter modeling in the state-space equation generated from (1)-(5) can be expressed as:

$$\boldsymbol{x}_{k+1} = \boldsymbol{A}\boldsymbol{x}_k + \boldsymbol{B}\boldsymbol{u}_k \tag{6}$$

$$\boldsymbol{x}_k = [V_o \quad \Delta i_{k,1} \quad \Delta i_{k,2} \quad \ldots \quad \Delta i_{k,n-1}]^{\mathrm{T}} \tag{7}$$

$$\boldsymbol{u}_k = [S_1 V_1 \quad S_2 V_2 \quad \ldots \quad S_n V_n]^{\mathrm{T}} \tag{8}$$

$$\boldsymbol{A} = \begin{bmatrix} 1 - T_s R_l\left(\frac{1}{L_1} + \frac{1}{L_2} + \ldots + \frac{1}{L_n}\right) & 0 & 0 & \ldots & 0 \\ T_s\left(\frac{\lambda_1}{L_2} - \frac{1}{L_1}\right) & 1 & 1 & \ldots & 1 \\ T_s\left(\frac{\lambda_2}{L_3} - \frac{1}{L_2}\right) & 1 & 1 & \ldots & 1 \\ \vdots & \vdots & \vdots & & \vdots \\ T_s\left(\frac{\lambda_{n-1}}{L_n} - \frac{1}{L_{n-1}}\right) & 1 & 1 & \ldots & 1 \end{bmatrix}_{n\times n} \tag{9}$$

$$\boldsymbol{B} = \begin{bmatrix} \frac{T_s R_l}{L_1} & \frac{T_s R_l}{L_2} & \frac{T_s R_l}{L_3} & \ldots & \frac{T_s R_l}{L_n} \\ \frac{T_s}{L_1} & -\frac{\lambda_1 T_s}{L_2} & 0 & \ldots & 0 \\ 0 & \frac{T_s}{L_2} & -\frac{\lambda_2 T_s}{L_3} & \ldots & 0 \\ \vdots & \vdots & \vdots & & \vdots \\ 0 & 0 & 0 & \ldots & -\frac{\lambda_{n-1} T_s}{L_n} \end{bmatrix}_{n\times n} \tag{10}$$

The measured output state is stated as:

$$\boldsymbol{y}_k=[V_o \quad \Delta i_{k,1} \quad \Delta i_{k,2} \quad \cdots \quad \Delta i_{k,n-1}]^{\mathrm{T}}\boldsymbol{H} \tag{11}$$

The parametric uncertainty is an approach used to represent a state-space equations with the parameter uncertainties of the system.

The two groups of uncertainties are classified as matched and unmatched uncertainties. This paper considers an unmatched uncertainty in the system using previously established procedures [21]. This model assumes that (6) has unmatched uncertainty in the system matrix (9) in the form of a discrete-time linear state-space representation as presented in (12).

$$\boldsymbol{x}_{k+1}=(\boldsymbol{A}+\Delta\boldsymbol{A}(L_{\mathrm{o}}))\boldsymbol{x}_k+\boldsymbol{B}\boldsymbol{u}_{ku} \tag{12}$$

An uncertainty component is split into the matched and unmatched uncertainties to solve the robust control problem. It is achieved using pseudo-inverse in the following form:

$$\boldsymbol{B}^{+}=(\boldsymbol{B}^{\mathrm{T}}\boldsymbol{B})^{-1}\boldsymbol{B}^{\mathrm{T}} \tag{13}$$

The unmatched uncertainty in the system (12) can be expressed as:

$$\Delta\boldsymbol{A}(L_o)=\boldsymbol{B}\boldsymbol{B}^{+}\Delta\boldsymbol{A}(L_o)+(\boldsymbol{I}-\boldsymbol{B}\boldsymbol{B}^{+})\Delta\boldsymbol{A}(L_o) \quad \forall L_o\in\Omega \tag{14}$$

The upper bound matrix component $\boldsymbol{\Gamma}>\boldsymbol{0}$ (for unmatched uncertainties) and $\boldsymbol{D}>\boldsymbol{0}$ (for matched uncertainties) are expressed in (15) and (16), respectively.

$$\varphi^{-1}(\Delta\boldsymbol{A}(L_o))^{\mathrm{T}}\Delta\boldsymbol{A}(L_o)\le\boldsymbol{\Gamma} \tag{15}$$

$$(\Delta\boldsymbol{A}(L_o))^{\mathrm{T}}(\boldsymbol{B}^{+})^{\mathrm{T}}\boldsymbol{B}^{+}\Delta\boldsymbol{A}(L_o)\le\boldsymbol{D} \tag{16}$$

where $\varphi\ge 0$.

Other types of DC/DC converters (boost and buck-boost) can also be derived from this modeling approach. The only difference is how the control input is selected. The current sharing is required to pass through the inductances of all types of DC/DC converters since they are assumed to operate in continuous-conduction mode [18]. Similarly, these DC/DC converters share the load current through inductance. As a result, inductance parametric uncertainty problems in all types of DC/DC converter topologies (buck, boost, and buck-boost) can be modeled similarly. This paper analyzes the inductive parametric uncertainties of DC/DC buck converters in islanded DC microgrid.

III. Description of Proposed Robust Control Strategy

In this section, the design procedure of the proposed robust control strategy is described using a system model (12). Figure 2 shows the overall structure of the proposed robust control strategy. Firstly, the robust state feedback control law needs to stabilize the DC-link voltage with unmatched uncertainty of the DC/DC converter inductance parameters with equal current sharing. Secondly, the controller gains are derived using the optimal control approach under UDARE. Lastly, the overall control input references to the cost function are generated to produce the gate signal to the converters. An integral action is added to eliminate error in the system. The control input is designed to stabilize all the states using a robust state feedback control law with unmatched parameter uncertainty as:

$$\boldsymbol{u}_r=\boldsymbol{K}_u\boldsymbol{x}_k \tag{17}$$

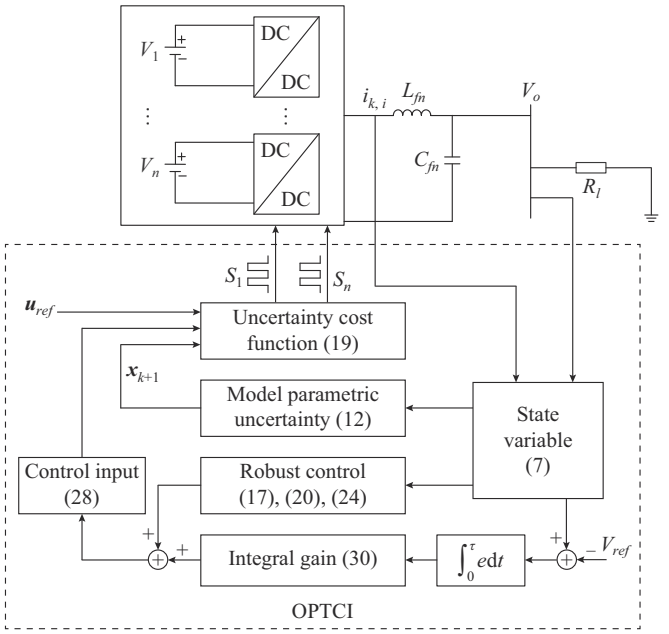

Fig. 2. Overall structure of proposed robust control strategy.

$\boldsymbol{K}_u$ can be designed in an optimal control approach such that the closed-loop of (12) is asymptotically stable, i. e., $\boldsymbol{y}_k\to\boldsymbol{x}_{ref}, \forall\Delta L_o\in\Omega$. The main idea for the optimal design control law is to compute $\boldsymbol{K}_u$. In this case, a nominal system (6) is presented with the help of virtual dynamic control input as previously formulated [19]:

$$\boldsymbol{x}_{k+1}=\boldsymbol{A}\boldsymbol{x}_k+\boldsymbol{B}\boldsymbol{u}_{ku}+\mu(\boldsymbol{I}-\boldsymbol{B}\boldsymbol{B}^{+})\boldsymbol{v}_k \tag{18}$$

The cost function, which minimizes the unmatched uncertainty parameter and ensures equal load current sharing, is expressed as:

$$J_u=\sum_{k=0}^{N}\left(\|\boldsymbol{x}_{k+1}\|_{\boldsymbol{S}_u}+\|\boldsymbol{x}_k\|_{\boldsymbol{Q}_u+\boldsymbol{\Gamma}+\beta^2\boldsymbol{I}}+\|\boldsymbol{u}_{ku}\|_{\boldsymbol{R}_u}+\|\boldsymbol{v}_k\|_{\boldsymbol{R}_u}\right)$$
$$\boldsymbol{Q}_u\ge\boldsymbol{0},\ \boldsymbol{R}_u>\boldsymbol{0},\boldsymbol{\Gamma}\ge\boldsymbol{0},\beta>0 \tag{19}$$

The above robust problem in (12) can be solved if the nominal system in (6) is controllable, and if both the design parameter $\varphi>0$ and the positive definite matrix $\boldsymbol{S}_u>\boldsymbol{0}$ (as a solution of UDARE) exist [19].

$$\boldsymbol{A}^{\mathrm{T}}[\boldsymbol{S}_u^{-1}+\boldsymbol{B}\boldsymbol{R}_u^{-1}\boldsymbol{B}^{\mathrm{T}}+\mu^2(\boldsymbol{I}-\boldsymbol{B}\boldsymbol{B}^{+})\boldsymbol{R}_u^{-1}(\boldsymbol{I}-\boldsymbol{B}\boldsymbol{B}^{+})^{\mathrm{T}}]^{-1}\boldsymbol{A}-$$
$$\boldsymbol{S}_u+\boldsymbol{Q}_u+\boldsymbol{\Gamma}+\beta^2\boldsymbol{I}=\boldsymbol{0} \tag{20}$$

$$\begin{cases}(\varphi^{-1}\boldsymbol{I}-\boldsymbol{S}_u)^{-1}>\boldsymbol{0}\\ \varphi^{-1}(\Delta\boldsymbol{A}(L_o))^{\mathrm{T}}\Delta\boldsymbol{A}(L_o)\le\boldsymbol{\Gamma}\end{cases} \tag{21}$$

The following constraint (22) is satisfied.

$$(\beta^2\boldsymbol{I}+\boldsymbol{L}_u^{\mathrm{T}}\boldsymbol{R}_u\boldsymbol{L}_u+\boldsymbol{K}_u^{\mathrm{T}}\boldsymbol{R}_u\boldsymbol{K}_u)-\boldsymbol{A}_u^{\mathrm{T}}(\boldsymbol{S}_u^{-1}-\varphi\boldsymbol{I})^{-1}\boldsymbol{A}_u\ge\boldsymbol{0} \tag{22}$$

where $\boldsymbol{A}_u=\boldsymbol{A}+\boldsymbol{B}\boldsymbol{K}_u$. There is a solution to the robust control problems of (12) that demonstrates the unmatched uncertainty controller gains as:

$$\begin{bmatrix} \boldsymbol{K}_u \\ \boldsymbol{L}_u \end{bmatrix} = \begin{bmatrix} -\boldsymbol{R}_u^{-1}\boldsymbol{B}^{\mathrm{T}} \\ -\varphi \boldsymbol{R}_u^{-1}(\boldsymbol{I}-\boldsymbol{B}\boldsymbol{B}^{+}) \end{bmatrix} [\boldsymbol{S}_u^{-1} + \boldsymbol{B}\boldsymbol{R}_u^{-1}\boldsymbol{B}^{\mathrm{T}} + \varphi^2 (\boldsymbol{I}-\boldsymbol{B}\boldsymbol{B}^{+})\boldsymbol{R}_u^{-1}(\boldsymbol{I}-\boldsymbol{B}\boldsymbol{B}^{+})^{\mathrm{T}}]^{-1}\boldsymbol{A} \quad (23)$$

$$\begin{bmatrix} \boldsymbol{u}_r \\ \boldsymbol{v}_k \end{bmatrix} = \begin{bmatrix} \boldsymbol{K}_u \\ \boldsymbol{L}_u \end{bmatrix} \boldsymbol{x}_k \quad (24)$$

The proof of (20) is presented in Appendix A using the following lemmas.

Lemma 1 Let $\boldsymbol{S}_u > \boldsymbol{0}$ be a definite positive solution of (20) with scalar $\varphi > 0$, which satisfies the following inequality:

$$\boldsymbol{A}_u^{\mathrm{T}}\boldsymbol{S}_u\Delta\boldsymbol{A}(L_o) + (\Delta\boldsymbol{A}(L_o))^{\mathrm{T}}\boldsymbol{S}_u\boldsymbol{A}_u + (\Delta\boldsymbol{A}(L_o))^{\mathrm{T}}\boldsymbol{S}_u\Delta\boldsymbol{A}(L_o) \le \boldsymbol{A}_u^{\mathrm{T}}\boldsymbol{S}_u(\varphi^{-1}\boldsymbol{I}-\boldsymbol{S}_u)^{-1}\boldsymbol{S}_u\boldsymbol{A}_u + \varphi^{-1}(\Delta\boldsymbol{A}(L_o))^{\mathrm{T}}\Delta\boldsymbol{A}(L_o) \quad (25)$$

where $(\varphi^{-1}\boldsymbol{I}-\boldsymbol{S}_u)^{-1} > \boldsymbol{0}$.

Lemma 2 Let $\boldsymbol{S}_u > \boldsymbol{0}$ be a solution to (20) that satisfies the following inequality:

$$\varphi^{-1}\boldsymbol{I} + \boldsymbol{S}_u(\varphi^{-1}\boldsymbol{I}-\boldsymbol{S}_u)^{-1}\boldsymbol{S}_u > \boldsymbol{0} \quad (26)$$

Furthermore, for the use of the robust controller gain in (23), the following inequality is satisfied.

$$\boldsymbol{A}_u^{\mathrm{T}}[\varphi^{-1}\boldsymbol{I} + \boldsymbol{S}_u(\varphi^{-1}\boldsymbol{I}-\boldsymbol{S}_u)^{-1}\boldsymbol{S}_u]\boldsymbol{A}_u - \boldsymbol{A}^{\mathrm{T}}[\boldsymbol{S}_u^{-1} + \boldsymbol{B}\boldsymbol{R}_u^{-1}\boldsymbol{B}^{\mathrm{T}} + \varphi^2(\boldsymbol{I}-\boldsymbol{B}\boldsymbol{B}^{+})\boldsymbol{R}_u^{-1}(\boldsymbol{I}-\boldsymbol{B}\boldsymbol{B}^{+})^{\mathrm{T}}]^{-1}\boldsymbol{A} \le \boldsymbol{A}_u^{\mathrm{T}}(\boldsymbol{S}_u^{-1}-\varphi^{-1}\boldsymbol{I})^{-1}\boldsymbol{A}_u - (\boldsymbol{L}_u^{\mathrm{T}}\boldsymbol{R}_u\boldsymbol{L}_u + \boldsymbol{K}_u^{\mathrm{T}}\boldsymbol{R}_u\boldsymbol{K}_u) \quad (27)$$

The overall control input is formulated as:

$$\boldsymbol{u}_{ku} = \boldsymbol{K}_i\xi_k + \boldsymbol{K}_u\boldsymbol{x}_k \quad (28)$$

Equation (28) is obtained by combining (17) with a control input of an integral action introduced to eliminate an error.

$$\boldsymbol{u}_{ki} = \boldsymbol{K}_i\xi_k \quad (29)$$

where $\xi_k = \int_0^{\tau} e\mathrm{d}t$ is a new variable generated by integral action, and its gain is also computed similarly using the pole-placement design approach as in [22].

$$\boldsymbol{K}_i = -(\boldsymbol{B}^{\mathrm{T}}\boldsymbol{B})^{-1}\boldsymbol{B}^{\mathrm{T}}(\boldsymbol{A} + \Delta\boldsymbol{A}(L_o) + \boldsymbol{B}\boldsymbol{K}_s) \quad (30)$$

As previously established in [23], the state variables and control input references are defined similarly.

$$\boldsymbol{x}_{ref} = [\boldsymbol{u}_{ku} \quad 0 \quad 0 \quad \dots \quad 0]^{\mathrm{T}} = \boldsymbol{x}_k = \boldsymbol{x}_{k+1} \quad (31)$$

$$\boldsymbol{u}_{ref} = [\boldsymbol{I} - (\boldsymbol{A} + \Delta\boldsymbol{A}(L_o))]\boldsymbol{B}^{-1}\boldsymbol{x}_{ref} \quad (32)$$

Lastly, the robust control input from (28) is designed to minimize (19) to generate the pulse width modulation (PWM) signals for the converter power switches, as illustrated in Fig. 2.

IV. Simulation and Experimental Results

A. Simulation Results and Discussion

The DC microgrid shown in Fig. 1 is implemented and simulated in the MATLAB/Simulink environment to validate the proposed robust control strategy. The simulation results are obtained using a base power of 1 MW from 2 kV DC sources, and a simple step-down DC-link voltage of 1 kV for all the DERs connected in parallel. Table I summarizes the simulation validation variables used. The robust control against parametric uncertainty is verified for a wide range of inductance parameter uncertainties with resistive load under equal current sharing. The simulation results with norminal paramters are depicted in Fig. 3.

TABLE I
Simulation Validation Variables

Variable	Value
V_{ref}	1 kV
$V_i\ (i=1,2,3)$	2 kV
$C_{ci}\ (i=1,2,3)$	50 μF
T_s	50 μs
R_l	1 Ω
$C_{fi}\ (i=1,2,3)$	80 nF
$L_{fi}\ (i=1,2,3)$	40 μH
$L_i\ (i=1,2,3)$	1 mH
F_s	20 kHz
L_o	≤3 mH

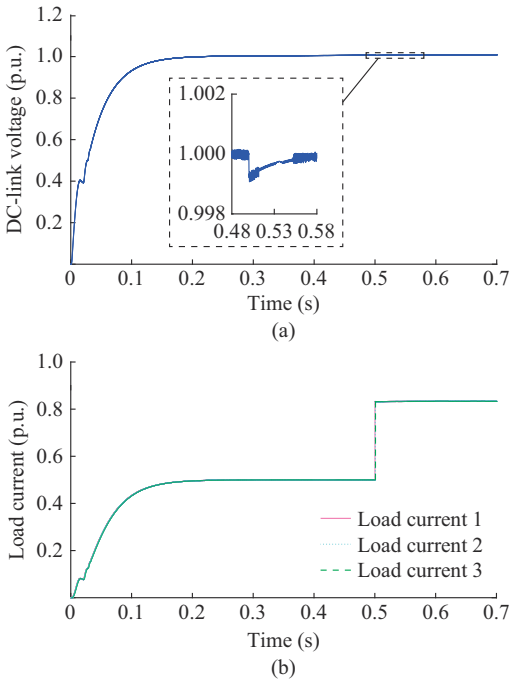

Fig. 3. Simulation results with nominal parameters. (a) DC-link voltage. (b) Load current.

The robustness and good performance of the proposed robust control strategy have been evaluated through uncertainties of the parallel DC/DC converter inductance parameter, as shown in Figs. 4(a), 5(a), and 6(a). For the purpose of illustrative comparison, the system has been simulated using a proportional-integral-derivative (PID) controller under the same operating conditions, as shown in Figs. 4(b), 5(b), and 6(b). The PID controller used in this case is based on the control structure from [10], and its tuning parameters are derived from the damping ratio of the converter and the undamping natural frequency of its transfer function as developed in [24].

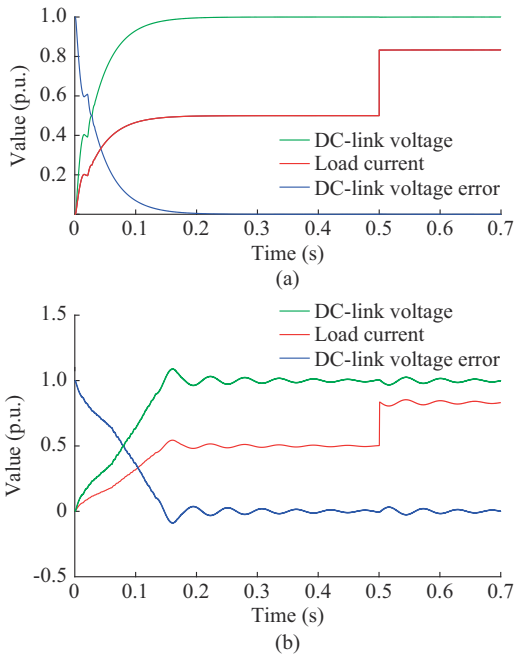

Fig. 4. Simulation results with L_o=1 mH. (a) OPTCI approach. (b) Traditional PID approach.

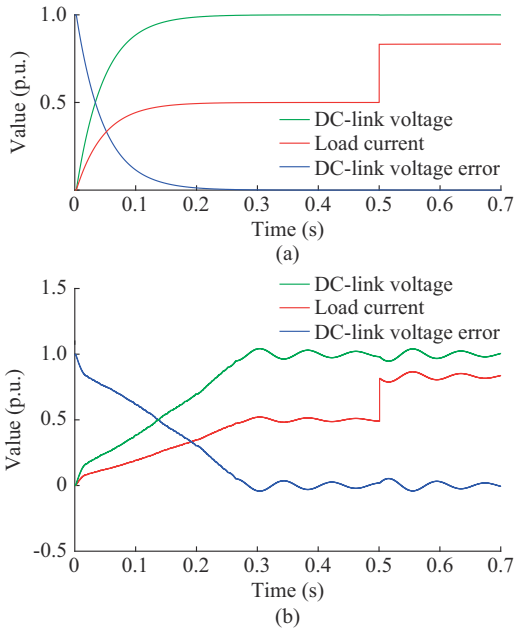

Fig. 5. Simulation results with L_o=2 mH. (a) OPTCI approach. (b) Traditional PID approach.

The parameters of the PID controller used in simulations are given as: K_i=1/100, K_p=1/100, K_d=3/100.

The results in Figs. 4-6 indicate that compared with the PID controller, the proposed robust control strategy provides better waveform quality under inductance parameter uncertainty. If the parameters in (9) and (10) are set to be L_n for scenario 1, then the parameter L_o increases for scenario 2. The values of L_o are increased again with an increase of resistive load at 0.5 s. The response characteristics are discussed below. In the case of selecting the inductance of the parallel DC/DC converter parameters at nominal values, a step change is applied after an increase of the resistive load at the DC-link voltage terminal. In Fig. 4, the inductance of the parallel DC/DC converter L_n is set to be L_n=L_o=1 mH. It can be observed from Fig. 4(a) that the OPTCI approach has zero overshoot on the DC-link voltage, better steady state on the load current, and precise zero-steady-state error on the DC-link voltage compared with the traditional PID approach in Fig. 4(b). Figure 5 shows the effect on the rising time when the parallel DC/DC converter inductance parameter is set to be L_o=2 mH. In Fig. 5(a), a fast rising time on DC-link voltage can be noted, and a strong anti-resistive load disturbance ability is observed on DC-link voltage steady-state error on the OPTCI approach compared with the PID approach shown in Fig. 5(b). A better overshoot is observed on the DC-link voltage steady-state error for the PID approach compared with the result shown in Fig. 4(b). Compared with the results of the OPTCI approach as shown in Fig. 6(a), the PID approach presented in Fig. 6(b) has a longer settling time, because the rising time is longer, proving that the proposed strategy is robust against inductance parametric uncertainty.

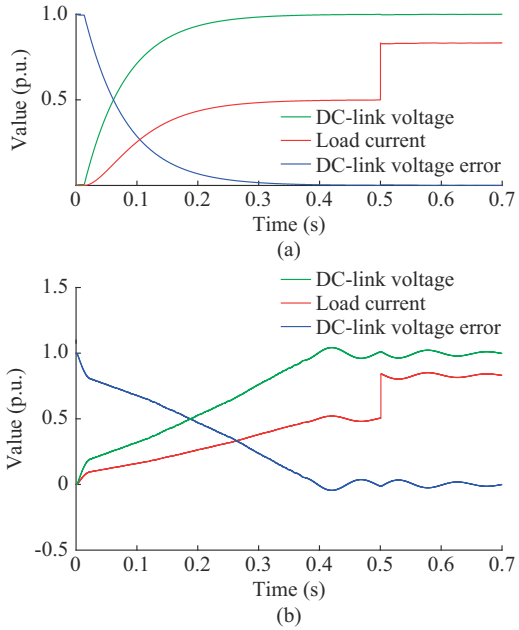

Fig. 6. Simulation results with L_o=3 mH. (a) OPTCI approach. (b) Traditional PID approach.

Figures 4-6 show the dynamic and steady-state performance of the OPTCI approach compared with the traditional PID approach, while Table II summarizes all of the results. The designs of PID and OPTCI approaches are based on the performance trade-off in practice, which is reflected directly from the turning of their bandwidth [25]. The amount of time spent in data exchange during the closed-loop operation to the sampling time is the bandwidth allocated to each closed-loop control. In the traditional PID approach, the bandwidth is used to adjust the DC-link voltage and guarantee the accuracy of current sharing by transferring output voltages and currents from various DC/DC converters. The OPTCI approach assigns bandwidth to each control loop based on the state of each DC/DC converter [26]. As de-

scribed in [26], when the DC microgrid is in equilibrium, a small bandwidth is required; however, when the DC microgrid is perturbed, an increase in the allocated bandwidth can accelerate the recovery of DC microgrid, enhancing the control performance via local bandwidth allocation.

TABLE II
COMPARISON PERFORMANCES OF OPTCI AND TRADITIONAL PID APPROACHES

Approach	L_o (mH)	ΔV_l (p.u.)	ΔV_o (p.u.)	t_s (ms)
OPTCI	1.00	0.0004	0	18
	2.00	0.0004	0	21
	3.00	0.0004	0	35
PID	1.00	0.0014	0	19
	2.00	0.0014	0	33
	3.00	0.0014	0	45

The simulation characteristic responses with OPTCI approach against inductive parametric uncertainty in DC microgrid is presented in Fig. 7. In this case, an uncertainty in DC/DC converter inductance L_o significantly affects the DC-link voltage error, DC-link voltage, and load current. The characteristic responses are summarized in Table III. A DC microgrid operates with three parallel DC/DC converters. From Fig. 7(a) and (b), it can be observed that the proposed robust control strategy ensures stability even under a wide range of inductance uncertainties with a characteristic response. The DC-link voltage overshoot is not noticeable with the decreasing converter inductance when the load is increased. However, the response of DC-link voltage droops is presented. The changes concerning the longer rising time of amplitude and settling time of load currents are needed, as shown in Fig. 7(c). If the converter inductance is larger than the nominal value ($L > L_n$), the oscillations will be larger than when it is less ($L < L_n$). In the following subsection, the effectiveness of the proposed strategy is validated in real time by observing the characteristics of the inductance uncertainties.

B. Experiment Validations and Analyses

A laboratory prototype of the testing system is used to verify the robustness of the proposed robust control strategy against inductance uncertainties of the DC/DC converters in real time. The hardware-in-loop system set-up is shown in Fig. 8. The proposed robust control strategy has been verified using the OpalRT real-time simulator OP5700, Lenovo central processor unit (CPU) model with an Intel Core i7 processor, in an HIL system. The HIL system consists of a compact Xilinx@Virtex 7-field programable gate array (FPGA)-based processor and fiber optic input/output (I/O) expansion unit. It provides the ability to validate DC microgrids in a flexible and non-destructive environment and quick prototyping. It has been used to build and compute a large-scale parallel calculation function with a tiny time step. According to the DC microgrid architecture, DERs and *n*-parallel DC/DC converters are operated as single entity through the mesurement of the DC-link voltage and inductance current sensors.

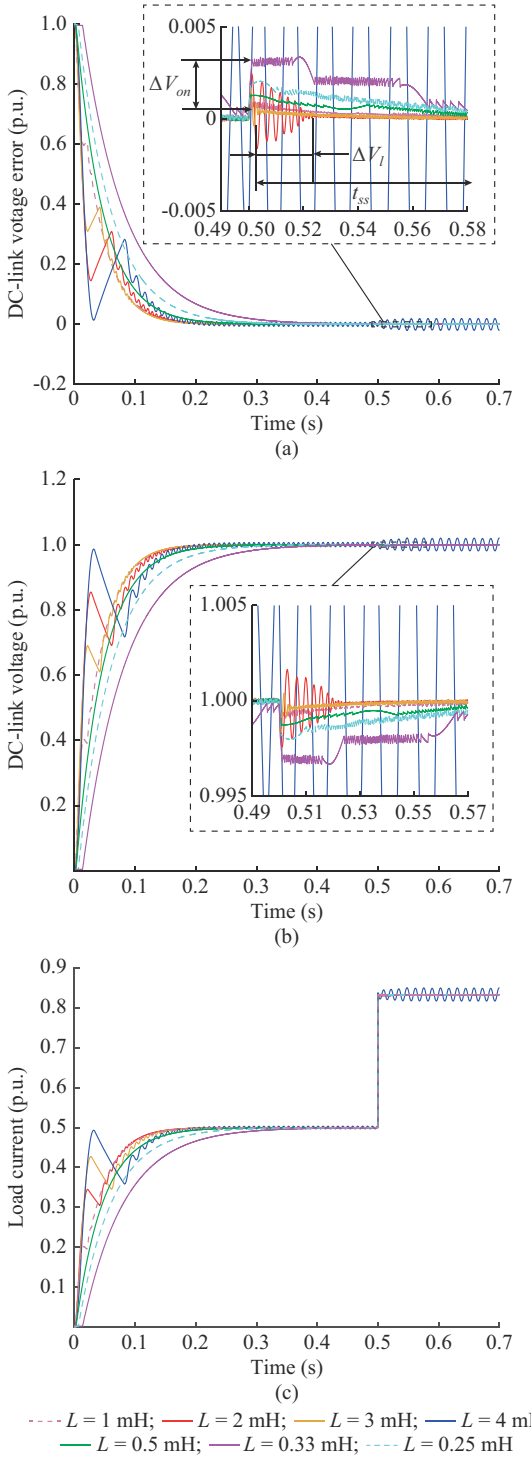

Fig. 7. Simulation characteristic responses with OPTCI approach against inductive parametric uncertainty. (a) DC-link voltage error. (b) DC-link voltage. (c) Load current.

TABLE III
CHARACTERISTIC RESPONSES OF DC-LINK VOLTAGE ERROR, DC-LINK VOLTAGE, AND LOAD CURRENT

L_o (mH)	ΔV_{op} (p.u.)	ΔV_l (p.u.)	ΔV_{osh} (p.u.)	t_s (ms)
2.00	0.0024	0.10	0	20
3.00	0.0017	0.10	0	23
0.50	0.0013	0.15	0	60
0.25	0.0032	0.30	0	62

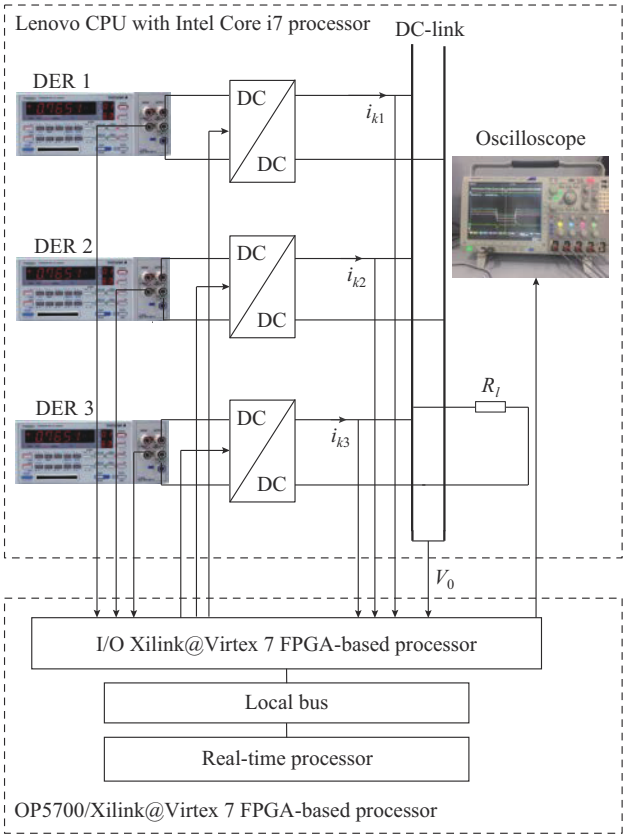

Fig. 8. Hardware-in-loop system set-up.

The real-time validation is conducted on a host personal computer (PC) running MATLAB/Simulink software, in which the DC microgrid model as well as the overall structure of the proposed robust control strategy in Fig. 2 is implemented. On the host PC, Simulink models are compiled into digital processing signal code, which is then loaded into the Xilinx@Virtex 7 FPGA-based processor. Artemis is an advanced 5-order technique used in an OpalRT library that interfaces with Simulink to generate state-space equation for the DC microgrid. The DC/DC parallel converter is theoretically modeled in FPGA with a set discrete-time step. The DC-link voltage, DC/DC converter inductance, and current sharing error are computed using the discrete-time step in the processor. Real-time validation is executed and recorded through the loopback I/O with a 20 kHz control frequency.

The parameter uncertainties of DC/DC converter inductances are observed with different values. The system responses are analyzed and compared with a traditional PID approach as performed in off-line validations. The real-time validation responses for the OPTCI approach and PID approach with different inductance values are depicted in Figs. 9 and 10, respectively. For $L_o = 0.25$ mH, it can be observed that the DC-link voltage responses with the OPTCI approach shown in Fig. 9 present a fast dynamic compared with the results obtained from the PID approach shown in Fig. 10. Excellent steady-state performance with the OPTCI approach can be easily observed, while oscillation appears when the PID approach is applied. The DC/DC converter inductances are also decreased for $L_o = 0.33$ mH. It can be observed from Fig. 10 that when the PID approach is applied, the rising time performance of the DC-link voltage response is increased. In addition, a large overshoot occurs in all inductance uncertainties, and the steady-state performance of the system will deteriorate with inductance uncertainties. The steady-state error of DC-link voltage with the OPTCI approach is reduced, whereas it is large when using the PID approach. In other words, by using the PID approach, the system characteristic is sensitive to the inductance parameter uncertainties and cause longer oscillations. However, with the proposed robust control strategy, better performances are obtained in both transient and steady states, proving that the OPTCI approach has strong robustness with a wide range of uncertainties of the DC/DC converter inductance.

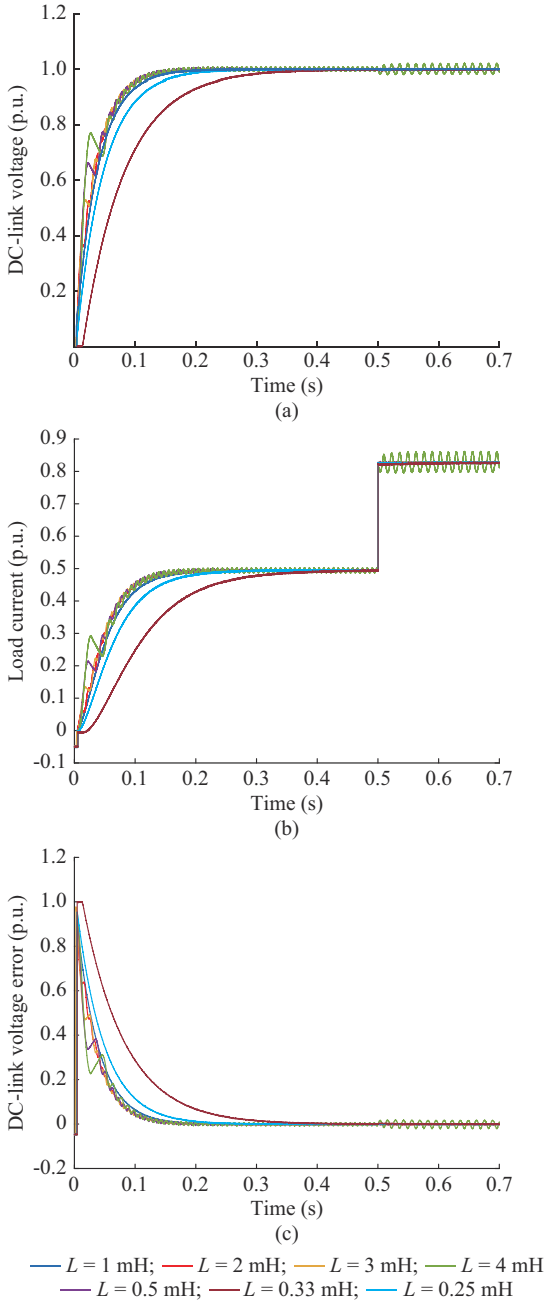

Fig. 9. Real-time validation responses for OPTCI approach with different inductance values. (a) DC-link voltage. (b) Load current. (c) DC-link voltage error.

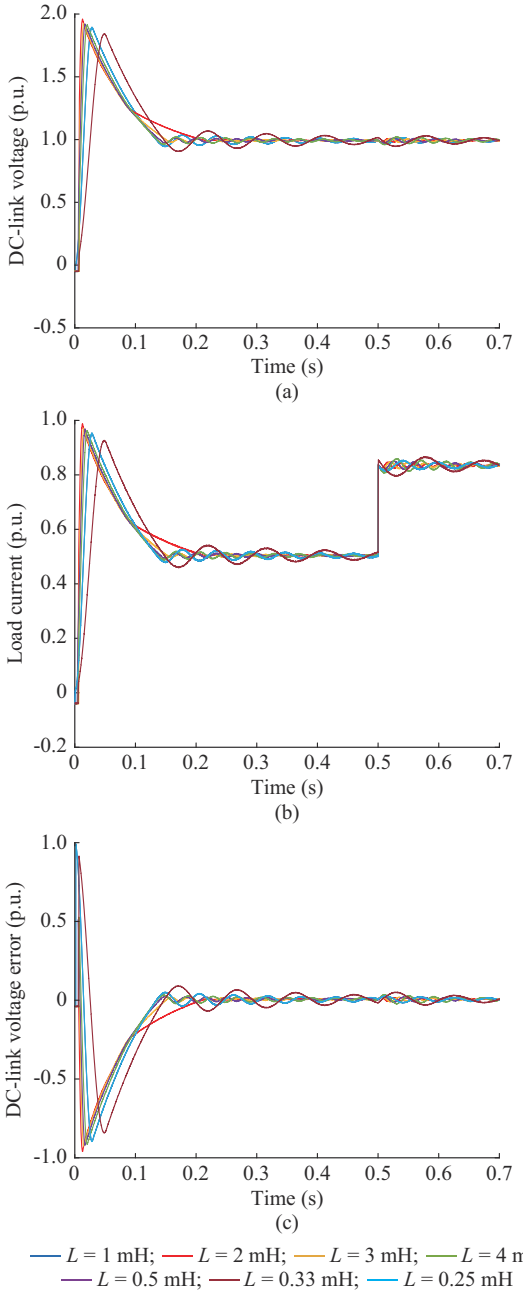

Fig. 10. Real-time validation responses for PID approach with different inductance values. (a) DC-link voltage. (b) Load current. (c) DC-link voltage error.

V. Conclusion

A robust control strategy to overcome uncertainty inductance parameters of DC/DC converters in islanded DC microgrid is proposed based on the OPTCI. The LQR, UDARE, and an integral action are applied in the state feedback loop to solve the parametric uncertainty problem. Such a combined control strategy allows for achieving a zero steady-state error on the DC-link voltage at any inductance parameter uncertainty with equal load current sharing capability. Intensive off-line and real-time simulations are conducted to validate the proposed robust control strategy. Off-line simulations are performed in MATLAB/Simulink environment, while the real-time validations are performed using the OpalRT simulator. In all the investigated cases, the effectiveness and suitability of the proposed robust control strategy for inductive parametric uncertainties are demonstrated by achieving improved operating performances of an islanded DC microgrid with multiple parallel DC/DC converters.

Appendix A

A fundamental part of this appendix is driven by the robust controller gain $\boldsymbol{K}_u$ with a virtual controller gain $\boldsymbol{L}_u$ to minimize (19) for the nominal system (18). For this purpose, the optimal control approaches for the unmatched uncertainty control input $\boldsymbol{u}_{ku}$ and virtual dynamic control input $\boldsymbol{v}_k$ should be minimized using the Hamiltonian approach as:

$$\begin{cases} \dfrac{\partial \boldsymbol{H}(\boldsymbol{x}_k, \boldsymbol{u}_{ku}, \boldsymbol{v}_k)}{\partial \boldsymbol{u}_{ku}} = \boldsymbol{0} \\ \dfrac{\partial \boldsymbol{H}(\boldsymbol{x}_k, \boldsymbol{u}_{ku}, \boldsymbol{v}_k)}{\partial \boldsymbol{v}_k} = \boldsymbol{0} \end{cases} \tag{A1}$$

By applying discrete-time LQR methods in (A1), the unmatched UDARE from (20) and that of robust controllers gain in (23) are achieved [27]. Since (9) and (10) are controllable matrices, the solution for the unmatched UDARE exists. From an unmatched uncertainty, state space (12) shows that the closed loop is stable asymptotically, as given by:

$$\begin{cases} \boldsymbol{x}_{k+1} = (\boldsymbol{A} + \Delta\boldsymbol{A}(L_o) + \boldsymbol{B}\boldsymbol{K}_u)\boldsymbol{x}_k \\ \boldsymbol{y}_k = \boldsymbol{H}\boldsymbol{x}_k \end{cases} \tag{A2}$$

where $\boldsymbol{y}_k \to \boldsymbol{x}_{ref}, \forall \Delta L_o \in \Omega$.

To verify the stability of the unmatched uncertainty system, let (A3) be an unmatched uncertainty Lyapunov function and use the time unmatched uncertainty increment of (A4) along with $\boldsymbol{x}_k$ and $\boldsymbol{A}_u = \boldsymbol{A} + \Delta\boldsymbol{A}(L_o) + \boldsymbol{B}\boldsymbol{K}_u$, such that:

$$V_u(\boldsymbol{x}_k) = \boldsymbol{x}_k^{\mathrm{T}} \boldsymbol{S}_u \boldsymbol{x}_k \tag{A3}$$

$$\begin{aligned} \Delta V_u = {} & \boldsymbol{x}_k^{\mathrm{T}} \boldsymbol{A}_u^{\mathrm{T}} \boldsymbol{S}_u \boldsymbol{A}_u \boldsymbol{x}_k + \boldsymbol{x}_k^{\mathrm{T}} \boldsymbol{A}_u^{\mathrm{T}} \boldsymbol{S}_u \Delta\boldsymbol{A}(L_o)\boldsymbol{x}_k + \boldsymbol{x}_k^{\mathrm{T}} \Delta\boldsymbol{A}(L_o) \boldsymbol{S}_u \boldsymbol{A}_u \boldsymbol{x}_k + \\ & \boldsymbol{x}_k^{\mathrm{T}} (\Delta\boldsymbol{A}(L_o))^{\mathrm{T}} \boldsymbol{S}_u \Delta\boldsymbol{A}(L_o)\boldsymbol{x}_k - \boldsymbol{x}_k^{\mathrm{T}} \boldsymbol{S}_u \boldsymbol{x}_k \end{aligned} \tag{A4}$$

By using the matrix inversion lemma, (A5) is achieved [28].

$$(\boldsymbol{S}_u^{-1} - \varphi \boldsymbol{I})^{-1} = \boldsymbol{S}_u + \boldsymbol{S}_u (\boldsymbol{S}_u^{-1} - \varphi \boldsymbol{I})^{-1} \boldsymbol{S}_u \tag{A5}$$

Using (20) and (A5) in (A4), (A6) is derived:

$$\begin{aligned} \Delta \boldsymbol{V}_u \le {} & \boldsymbol{x}_k^{\mathrm{T}} \{ \boldsymbol{A}_u^{\mathrm{T}} (\boldsymbol{S}_u^{-1} - \varphi \boldsymbol{I})^{-1} \boldsymbol{A}_u - \boldsymbol{Q}_u - \beta^2 \boldsymbol{I} - \boldsymbol{A}_u^{\mathrm{T}} [\boldsymbol{S}_u^{-1} + \\ & \boldsymbol{B}\boldsymbol{R}_u^{-1} \boldsymbol{B}^{\mathrm{T}} + \varphi^2 (\boldsymbol{I} - \boldsymbol{B}\boldsymbol{B}^{+}) \boldsymbol{R}_u^{-1} (\boldsymbol{I} - \boldsymbol{B}\boldsymbol{B}^{+})^{\mathrm{T}}]^{-1} \boldsymbol{A} \} \boldsymbol{x}_k - \\ & \boldsymbol{x}_k^{\mathrm{T}} (\boldsymbol{\Gamma} - \varphi^{-1} (\Delta\boldsymbol{A}(L_o))^{\mathrm{T}} \Delta\boldsymbol{A}(L_o)) \boldsymbol{x}_k \end{aligned} \tag{A6}$$

Inequality (A6) is simplified with Lemmas 1 and 2 as:

$$\Delta \boldsymbol{V}_u \le -\boldsymbol{x}_k^{\mathrm{T}} [(\beta^2 \boldsymbol{I} + \boldsymbol{L}_u^{\mathrm{T}} \boldsymbol{R}_u \boldsymbol{L}_u + \boldsymbol{K}_u^{\mathrm{T}} \boldsymbol{R}_u \boldsymbol{K}_u) - \boldsymbol{A}_u^{\mathrm{T}} (\boldsymbol{S}_u^{-1} - \varphi \boldsymbol{I})^{-1} \boldsymbol{A}_u] \boldsymbol{x}_k \tag{A7}$$

Inequality (A7) is negative semi-definite if and only if (22) is satisfied. Therefore, from the Lyapunov practical stability theory, the closed-loop unmatched uncertainty of (A2) is stable for $\forall \Delta L_o \in \Omega$ [19].

References

[1] J. Kumar, A. Agarwal, and V. Agarwal, "A review on overall control

of DC microgrids," *Journal of Energy Storage*, vol. 21, pp. 113-138, Feb. 2019.
[2] R. K. Chauhan and K. Chauhan, *Distributed Energy Resources in Microgrids*. Amsterdam: Elsevier, 2019.
[3] K. Bharath, M. M. Krishnan, and P. Kanakasabapathy, "A review on DC microgrid control techniques applications and trends," *International Journal of Renewable Energy Research (IJRER)*, vol. 9, no. 3, pp. 1328-1338, Sept. 2019.
[4] U. Vuyyuru, S. Maiti, and C. Chakraborty, "Active power flow control between DC microgrids," *IEEE Transactions on Smart Grid*, vol. 10, no. 6, pp. 5712-5723, Nov. 2019.
[5] X. Lu, J. M. Guerrero, K. Sun *et al.*, "An improved droop control method for DC microgrids based on low bandwidth communication with DC bus voltage restoration and enhanced current sharing accuracy," *IEEE Transactions on Power Electronics*, vol. 29, no. 4, pp. 1800-1812, Apr. 2014.
[6] C. Papadimitriou, E. Zountouridou, and N. Hatziargyriou, "Review of hierarchical control in DC microgrids," *Electric Power Systems Research*, vol. 122, pp. 159-167, May 2015.
[7] K. Wang, X. Huang, B. Fan *et al*., "Decentralized power sharing control for parallel-connected inverters in islanded single-phase microgrids," *IEEE Tranactions on Smart Grid*, vol. 9, no. 6, pp. 6721-6730, Nov. 2018.
[8] A. Khorsandi, M. Ashourloo, and H. Mokhtari, "A decentralized control method for a low-voltage DC microgrid," *IEEE Transactions on Energy Conversion*, vol. 29, no. 4, pp. 793-801, Dec. 2014.
[9] M. Mokhtar, M. I. Marei, and A. A. El-Sattar, "An adaptive droop control scheme for DC microgrids integrating sliding mode voltage and current controlled boost converters," *IEEE Transactions on Smart Grid*, vol. 10, no. 2, pp. 1685-1693, Mar. 2019.
[10] S. Anand, B. G. Fernandes, and J. Guerrero, "Distributed control to ensure proportional load sharing and improve voltage regulation in low-voltage DC microgrids," *IEEE Transactions on Power Electronics*, vol. 28, no. 4, pp. 1900-1913, Apr. 2013.
[11] P. Wang, X. Lu, X. Yang *et al*., "An improved distributed secondary control method for DC microgrids with enhanced dynamic current sharing performance," *IEEE Transactions on Power Electronics*, vol. 31, no. 9, pp. 6658-6673, Sept. 2016.
[12] P.-H. Huang, P.-C. Liu, W. Xiao *et al*., "A novel droop-based average voltage sharing control strategy for DC microgrids," *IEEE Transactions on Smart Grid*, vol. 6, no. 3, pp. 1096-1106, May 2015.
[13] C. Wang, J. Duan, B. Fan *et al*., "Decentralized high-performance control of DC microgrids," *IEEE Transactions on Smart Grid*, vol. 10, no. 3, pp. 3355-3363, May 2019.
[14] Z. Yi, X. Zhao, D. Shi *et al*., "Accurate power sharing and synthetic inertia control for DC building microgrids with guaranteed performance," *IEEE Access*, vol. 7, pp. 63698-63708, May 2019.
[15] R. Han, L. Meng, J. M. Guerrero *et al*., "Distributed nonlinear control with event-triggered communication to achieve current-sharing and voltage regulation in DC microgrids," *IEEE Transactions on Power Electronics*, vol. 33, no. 7, pp. 6416-6433, Jul. 2018.
[16] S. Adhikar, Q. Xu, Y. Tang *et al*., "Decentralized control of two DC microgrids interconnected with tie-line," *Journal of Modern Power Systems and Clean Energy*, vol. 5, no. 4, pp. 599-608, Jul. 2017.
[17] S Aatif, H. Hu, X. Yang *et al.*, "Adaptive droop control for better current-sharing in VSC-based MVDC railway electrification system," *Journal of Modern Power Systems and Clean Energy*, vol. 7, no. 4, pp. 962-974, Jul. 2019.
[18] M. Baranwal, A. Askarian, S. Salapaka *et al.*, "A distributed architecture for robust and optimal control of DC microgrids," *IEEE Transactions on Industrial Electronics*, vol. 66, no. 4, pp. 3082-3092, Apr. 2019.
[19] N. S. Tripathy, I. Kar, and K. Paul, "Stabilization of uncertain discrete-time linear system via limited information," *IEEE Transactions on Automatic Control*, vol. 62, no. 9, pp. 4727-4733, Sept. 2017.
[20] F. Habibi, A. H. Naghshbandy, and H. Bevrani, "Robust voltage controller design for an isolated microgrid using Kharitonov's theorem and *D*-stability concept," *Internatioanl Jouranl of Electrical Power and Energy Systems*, vol. 44, no. 1, pp. 656-665, Jan. 2013.
[21] F. Lin, *Robust Control Design: an Optimal Control Approach.* Hoboken: Wiley & Sons, 2007.
[22] M. Muhammad, A. M. Abdullahi, A. A. Bature *et al.*, "LMI-based control of a double pendulum crane," *Applications of Modelling and Simulation*, vol. 2, pp. 41-50, Sept. 2018.
[23] R. P. Aguilera and D. E. Quevedo, "Predictive control of power converters: designs with guaranteed performance," *IEEE Transactions on Industrial Informatics*, vol. 11, no. 1, pp. 53-63, Feb. 2015.
[24] F. A. Salem and A. A. Rashed, "PID controllers and algorithms: selection and design techniques applied in mechatronics systems design – part II," *International Journal of Engineering Sciences*, vol. 2, no. 5, pp. 191-203, May 2013.
[25] Z. Gao, "Scaling and bandwidth-parameterization based controller tuning," in *Proceedings of the American Control Conference*, Denver, USA, Jun. 2003, pp. 4989-4996.
[26] M. Velasco, J. M. Fuertes, C. Lin *et al*., "A control approach to bandwidth management in networked control systems," in *Proceedings of the 30th Annual Conference of IEEE Industrial Electronics Society (IECON)*, Busan, South Korea, Nov. 2004, pp. 2343-2348.
[27] D. S. Naidu, *Optimal Control Systems*. Boca Raton: CRC Press, 2003.
[28] R. A. Horn and C. R. Johnson, *Matrix Analysis*. Cambridge: Cambridge University Press, 1994.

Salisu Abdullahi received the B.Eng. and M.S. degrees from the Electrical Engineering Department, Kano University of Science and Technology Wudil, Kano, Nigeria, and the Electrical-Electronics Engineering Department, Yasar University, Izmir, Turkey, in 2010 and 2015, respectively. He is currently working toward the Ph.D. degree with the Collage of Electrical Engineering and Automation, Fuzhou University, Fuzhou, China. His research interests include applications of robust control, optimal control, and model predictive control in DC/AC microgrids.

Tao Jin received the B.S. and M.S. degrees in electrical engineering from Yanshan University, Qinhuangdao, China, in 1998 and 2001, respectively, and the Ph.D. degree in electrical engineering from Shanghai Jiao Tong University, Shanghai, China, in 2005. From 2005 to 2007, he worked as a Postdoctor in Shanghai Jiao Tong University. During this time, he was in charge of a research group in the biggest dry-type transformer company in Asia, Sunten Electrical Co., Ltd., to develop new transformer technology with distribution grid. From 2008 to 2009, he held research scientist position with Virginia Tech, Blacksburg, USA. In 2010, he joined Imperial College London, London, UK, as an European Union Marie Curie Research Fellow. He is currently a Professor in College of Electrical Engineering and Automation, Fuzhou University, Fuzhou, China. He has published about 180 papers, and he is member of IEEE Power and Energy Society and IEEE Industrial Electronics Society, and Special Committee Member of Chinese Society of Electrical Engineering, China Electrotechnical Society, etc. He currently serves as Associate Editors for Journal of Modern Power Systems and Clean Energy, Protection and Control of Modern Power Systems, China Measurement & Testing Technology, and other journals. His research interests include power grid analysis, power electronics, and signal processing.

P. M. Lingom received the B.S. and M.S. degrees in pedagogical sciences and electrical engineering from the University of Douala, Douala, Cameroon, in 2014 and 2016, respectively. He is currently working toward the Ph.D. degree with the College of Electrical Engineering and Automation, Fuzhou University, Fuzhou, China. His research interests include analysis and control of multilevel power converters, and theoretical understanding of effects of variable frequency drive (VFD) induced harmonics in rotating machinery systems, as well as control of renewable energy systems.